

Universität des Saarlandes



Fachrichtung 6.1 – Mathematik

Preprint Nr. 224

**On the impact of the scheme for solving the  
higher-dimensional equation in coupled  
population balance systems**

Volker John and Michael Roland

Saarbrücken 2008



# On the impact of the scheme for solving the higher-dimensional equation in coupled population balance systems

**Volker John**

Saarland University  
Department of Mathematics  
P.O. Box 15 11 50  
66041 Saarbrücken  
Germany  
`john@math.uni-sb.de`

**Michael Roland**

Saarland University  
Department of Mathematics  
P.O. Box 15 11 50  
66041 Saarbrücken  
Germany  
`michael.roland@math.uni-sb.de`

Edited by  
FR 6.1 – Mathematik  
Universität des Saarlandes  
Postfach 15 11 50  
66041 Saarbrücken  
Germany

Fax: + 49 681 302 4443  
e-Mail: [preprint@math.uni-sb.de](mailto:preprint@math.uni-sb.de)  
WWW: <http://www.math.uni-sb.de/>

## Abstract

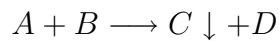
Population balance systems are models for processes in nature and industry which lead to a coupled system of equations (Navier–Stokes equations, transport equations, ...) where the equations are defined in domains with different dimensions. This paper will study the impact of using different schemes for solving the three–dimensional equation of a precipitation process in a two–dimensional flow domain. The numerical schemes for the three–dimensional equation are assessed with respect to the median of the volume fraction of the particle size distribution and the computational costs. It turns out that in the case of a structured flow field with small variations in time all schemes give qualitatively the same results. For a highly time–dependent flow field, the evolution of the median of the volume fraction differs considerably between first order and higher order schemes.

## 1 Introduction

Modern computers offer the possibility of simulating problems coming from nature or applications which are modeled by coupled systems of equations with increasing complexity. Typical examples are population balance systems. These systems describe the behavior of populations, e.g. of particles, by means of population balance equations, e.g. for the particle size distribution. An example is the droplet size distribution in clouds which is modeled with a population balance system [31]. This example already shows some difficulties which might be connected to the simulation of population balance systems: generally the droplets are driven by a turbulent flow and scales of very different sizes occur in this problem.

From the point of view of simulations, there is another challenge: the particle size distributions depend not only on space and time, like e.g. the velocity of the flow field, but they depend also on properties of the particles, so–called internal coordinates. Consequently, the population balance equation is defined in a higher dimensional domain than the other equations in the population balance system. The different dimensions of the equations in the population balance system will influence the numerical schemes which should be used. Schemes which are accurate and efficient for the equations defined in the space–time domain might become inefficient for the equations defined in the higher dimensional domain (curse of dimension). It could be advisable to use instead inexpensive schemes for these equations. However, the higher efficiency of these schemes will result generally in more inaccurate solutions. It has to be studied if the gains in the efficiency justify the losses in the accuracy. This paper will present investigations of this topic.

The considered model problem in this paper is the simulation of a precipitation process since this kind of process is rather well understood. In addition, it is much simpler than e.g. the simulation of clouds. The flows in precipitation processes are often laminar, breakage and agglomeration of particles are of minor importance and can be neglected. Precipitation processes are widely used in the chemical industry for producing particles with prescribed properties. They are modeled by population balance systems consisting of equations describing the flow field (Navier–Stokes equations), equations for the chemical reaction (convection–diffusion–reaction equations) and an equation for the particle size distribution (PSD, transport equation). In the basic form of a precipitation process, a chemical reaction



occurs in the liquid phase. The initially dissolved product  $C$  starts to precipitate, i.e. the nucleation of particles starts, if its local concentration exceeds the saturation concentration. Functionals of the distribution of particles, in particular at the outlet of the chemical device, are of primary interest in applications.

There are only initial attempts to simulate the population balance system describing a precipitation process [5, 16, 19, 20, 30]. The present paper will study the example from [16]. This example describes a calcium carbonate precipitation in a cavity. The modeling assumptions are such that on the one hand some properties of the actual process are simplified. On the other hand, the arising coupled system of equations is still so complex that severe difficulties in the simulations, using some standard numerical methods, have been reported in [16]. For completeness of presentation, the modeling assumptions are repeated here:

- the flow is two–dimensional, incompressible and laminar,
- the chemical reaction is isothermal,
- the PSD depends on one internal coordinate, namely the size of the particles,
- the particles, resp. the PSD, do not affect the flow field since their concentration is small,
- the particles follow the streamlines of the flow field because of their small size,

- nucleation and growth of particles, which are the most important phenomena governing the process of particle precipitation, are included into the model; agglomeration and breakage of particles are neglected.

From these assumptions, it follows that the flow field can be simulated independently of the chemical reaction and the precipitation process. The coupled system of equations describing the precipitation process based on these assumptions is given in Section 2.

A main difficulty of the simulations presented in [16] was the solution of the equations describing the chemical reaction. The simulation of such equations has been studied meanwhile separately in [17, 18]. In these studies, much better methods than the standard schemes used in [16] could be identified, see Section 3.2 for details. We will use one of these better methods in the numerical studies presented in this paper.

The main focus of this paper is on the simulation of the equation describing the PSD. From the modeling assumptions it follows that this equation is given in a 3D domain whereas the other equations are given in a 2D domain. For this reason, the solution of the transport equation for the PSD is potentially much more expensive than the solution of the other equations. One feels tempt to apply for this equation a comparatively cheap method, thereby accepting losses in the accuracy of the PSD solution. The main goal of this paper will be the study of the efficiency of several methods which can be used for simulating the PSD equation and on their effect to an output functional which is of interest in applications. To our best knowledge, such studies are not yet available, at least not for the simulation of precipitation processes.

The paper is organized as follows: Section 2 provides the model of the precipitation process leading to the dimensionless population balance system which is solved in the simulations. The numerical methods used in these simulations are described in Section 3. Numerical simulations are presented in Section 4. Two situations will be considered: a structured flow field with only small variations in time and a highly time-dependent process. The main results of the numerical studies are summarized in Section 5.

## 2 The population balance system for the precipitation process

The behavior of incompressible flows is modeled by the incompressible Navier–Stokes equations

$$\frac{\partial \tilde{\mathbf{u}}}{\partial \tilde{t}} - \nu \Delta \tilde{\mathbf{u}} + (\tilde{\mathbf{u}} \cdot \nabla) \tilde{\mathbf{u}} + \frac{1}{\rho} \nabla \tilde{p} = \mathbf{0} \text{ in } (0, \tilde{T}] \times \tilde{\Omega}, \quad (1)$$

$$\nabla \cdot \tilde{\mathbf{u}} = 0 \text{ in } [0, \tilde{T}] \times \tilde{\Omega}, \quad (2)$$

where  $\tilde{\mathbf{u}}$  [ $m/s$ ] denotes the fluid velocity,  $\tilde{p}$  [ $kg/(m \ s^2)$ ] the pressure,  $\nu$  [ $m^2/s$ ] the kinematic viscosity,  $\rho$  [ $kg/m^3$ ] the density,  $\tilde{\Omega}$  the flow domain and  $\tilde{T}$  [ $s$ ] the end of a time interval. In the precipitation process considered in this paper, the influence of the particles onto the flow field can be neglected since both, the size and the number of particles, will be sufficiently small. Thus (1), (2) govern the flow field of the precipitation process.

The concentrations of the dissolved substances  $A, B$  and  $C$  will be denoted by  $\tilde{c}_i$  [ $kmol/m^3$ ],  $i \in \{A, B, C\}$ . The concentrations of the reactants  $A$  and  $B$  obey a system of nonlinear convection–diffusion–reaction equations

$$\frac{\partial \tilde{c}_i}{\partial \tilde{t}} - D_i \Delta \tilde{c}_i + \tilde{\mathbf{u}} \cdot \nabla \tilde{c}_i + \tilde{r}_{\text{chem}}(\tilde{c}_A, \tilde{c}_B) = 0 \text{ in } (0, \tilde{T}] \times \tilde{\Omega}, \quad i \in \{A, B\}, \quad (3)$$

where  $D_i$  [ $m^2/s$ ] denotes the diffusion coefficient of  $A$  and  $B$ . The rate of the chemical reaction  $\tilde{r}_{\text{chem}}(\tilde{c}_A, \tilde{c}_B)$  [ $kmol/(m^3 \ s)$ ] is given by

$$\tilde{r}_{\text{chem}}(\tilde{c}_A, \tilde{c}_B) = k_R \tilde{c}_A \tilde{c}_B,$$

with the rate–constant  $k_R$  [ $m^3/(kmol \ s)$ ]. The reaction of  $A$  and  $B$  is modeled to be independent of the dissolved and the solid product  $C$ .

The dissolved product  $C$  satisfies the following equation

$$\begin{aligned} \frac{\partial \tilde{c}_C}{\partial \tilde{t}} - D_C \Delta \tilde{c}_C + \tilde{\mathbf{u}} \cdot \nabla \tilde{c}_C - \tilde{r}_{\text{chem}}(\tilde{c}_A, \tilde{c}_B) \\ + \tilde{r}_{\text{nuc}}(\tilde{c}_C) + \tilde{r}_g(\tilde{c}_C, \tilde{f}) = 0 \text{ in } (0, \tilde{T}] \times \tilde{\Omega}, \end{aligned}$$

with the diffusion coefficient  $D_C$  [ $m^2/s$ ]. The last three terms on the left–hand side describe, respectively, the production of dissolved  $C$ , the consumption of dissolved  $C$  caused by the nucleation of particles, and the consumption of dissolved  $C$  caused by the growth of particles. The rate of decrease of  $\tilde{c}_C$  due to the nucleation  $\tilde{r}_{\text{nuc}}(\tilde{c}_C)$  [ $kmol/(m^3 \ s)$ ] is given by

$$\tilde{r}_{\text{nuc}}(\tilde{c}_C) = C_{\text{nuc}} \tilde{d}_{p,0}^3 \tilde{B}_{\text{nuc}}(\tilde{c}_C),$$

where  $C_{\text{nuc}} [kmol/m^3]$  is a model nucleation constant,  $\tilde{d}_{p,0} [m]$  denotes the smallest particle diameter (the nuclei size), and the nucleation rate  $\tilde{B}_{\text{nuc}}(\tilde{c}_C)$  [ $1/(m^3 s)$ ] is defined by

$$\tilde{B}_{\text{nuc}}(\tilde{c}_C) = \max \left\{ k_{\text{nuc}} \left( \tilde{c}_C - c_{C,\infty}^{\text{sat}} \exp \left( \frac{C_2}{\tilde{d}_{p,0}} \right) \right)^5, 0 \right\},$$

see [27]. Here,  $k_{\text{nuc}} [(1/(m^3 s))/(kmol/m^3)^5]$  is the nucleation constant,  $c_{C,\infty}^{\text{sat}} [kmol/m^3]$  denotes the saturation concentration of the dissolved product  $C$  and  $C_2 [m]$  is a model constant. The rate of decrease of  $\tilde{c}_C$  due to the growth of the particles  $\tilde{r}_g(\tilde{c}_C, \tilde{f}) [kmol/(m^3 s)]$  is given by

$$\tilde{r}_g(\tilde{c}_C, \tilde{f}) = C_G \int_{\tilde{d}_{p,0}}^{\tilde{d}_{p,\text{max}}} \tilde{G}(\tilde{c}_C) \tilde{d}_p^2 \tilde{f} d(\tilde{d}_p),$$

where  $C_G [kmol/m^3]$  denotes a growth constant,  $\tilde{d}_{p,\text{max}} [m]$  is an upper bound for the particle diameter,  $\tilde{d}_p [m]$  the particle diameter and  $\tilde{f}(\tilde{t}, \tilde{\mathbf{x}}, \tilde{d}_p) [1/m^4]$  is the PSD. The growth rate  $\tilde{G}(\tilde{c}_C) [m/s]$  is considered to be independent of the size of the particles and, similar to the one in [7], given by

$$\tilde{G}(\tilde{c}_C) = k_G (\tilde{c}_C - c_{C,\infty}^{\text{sat}}),$$

where  $k_G [m^4/(kmol s)]$  is the growth rate constant. If  $\tilde{c}_C < c_{C,\infty}^{\text{sat}}$  and  $k_G > 0$ , particles might be dissolved again.

The product  $D$  is not simulated since it is not of interest for the precipitation process.

Finally, the higher-dimensional equation for the PSD is given by

$$\frac{\partial \tilde{f}}{\partial \tilde{t}} + \tilde{\mathbf{u}} \cdot \nabla \tilde{f} + \tilde{G}(\tilde{c}_C) \frac{\partial \tilde{f}}{\partial \tilde{d}_p} = 0 \text{ in } (0, \tilde{T}] \times \tilde{\Omega} \times (\tilde{d}_{p,0}, \tilde{d}_{p,\text{max}}). \quad (4)$$

For completeness of description, the derivation of the dimensionless equations for the simulations is given briefly. Let

$$\mathbf{u} = \frac{\tilde{\mathbf{u}}}{u_\infty}, \quad p = \frac{\tilde{p}}{p_\infty}, \quad t = \frac{\tilde{t}}{t_\infty}, \quad x_i = \frac{\tilde{x}_i}{l_\infty} \quad (i = 1, 2) \quad (5)$$

be dimensionless variables. Substituting them into (1), (2), multiplying the equation of the momentum balance by  $l_\infty/u_\infty^2$  and setting the time and pressure scales to

$$t_\infty = \frac{l_\infty}{u_\infty}, \quad p_\infty = \rho u_\infty^2,$$

the dimensionless Navier–Stokes equations

$$\frac{\partial \mathbf{u}}{\partial t} - \frac{1}{Re} \Delta \mathbf{u} + (\mathbf{u} \cdot \nabla) \mathbf{u} + \nabla p = \mathbf{0} \text{ in } (0, T] \times \Omega, \quad (6)$$

$$\nabla \cdot \mathbf{u} = 0 \text{ in } [0, T] \times \Omega, \quad (7)$$

are obtained, where  $Re = u_\infty l_\infty / \nu$  is the Reynolds number and  $T = \tilde{T} / t_\infty$ . Defining the dimensionless concentrations by  $c_i = \tilde{c}_i / c_\infty$ ,  $i \in \{A, B\}$ , substituting  $\tilde{c}_i$  into (3) and multiplying with  $l_\infty / (c_\infty u_\infty)$  lead to equations for the dimensionless reactants  $A$  and  $B$

$$\frac{\partial c_i}{\partial t} - \frac{D_i}{u_\infty l_\infty} \Delta c_i + \mathbf{u} \cdot \nabla c_i + k_R \frac{l_\infty c_\infty}{u_\infty} c_A c_B = 0 \text{ in } (0, T] \times \Omega. \quad (8)$$

In a similar way, using the dimensionless variables

$$c_C = \frac{\tilde{c}_C}{c_{C,\infty}}, \quad f = \frac{\tilde{f}}{f_\infty}, \quad d_p = \frac{\tilde{d}_p}{d_{p,\infty}}$$

and the scales

$$c_{C,\infty} = c_{C,\infty}^{\text{sat}} \exp\left(\frac{C_2}{\tilde{d}_{p,0}}\right), \quad d_{p,\infty} = \tilde{d}_{p,\text{max}}, \quad f_\infty = \frac{u_\infty}{C_G k_G d_{p,\infty}^3 l_\infty}, \quad (9)$$

the dimensionless equation for the concentration of the dissolved product  $C$  is obtained:

$$\begin{aligned} \frac{\partial c_C}{\partial t} - \frac{D_C}{u_\infty l_\infty} \Delta c_C + \mathbf{u} \cdot \nabla c_C - \Lambda_{\text{chem}} c_A c_B + \Lambda_{\text{nuc}} \max\{0, (c_C - 1)^5\} \\ + \left(c_C - \frac{c_{C,\infty}^{\text{sat}}}{c_{C,\infty}}\right) \int_{d_{p,\text{min}}}^1 d_p^2 f d(d_p) = 0 \text{ in } (0, T] \times \Omega. \end{aligned} \quad (10)$$

The constants in (10) are

$$\Lambda_{\text{chem}} = k_R \frac{c_\infty^2 l_\infty}{c_{C,\infty} u_\infty}, \quad d_{p,\text{min}} = \frac{\tilde{d}_{p,0}}{d_{p,\infty}}, \quad \Lambda_{\text{nuc}} = C_{\text{nuc}} d_{p,\text{min}}^3 d_{p,\infty}^3 k_{\text{nuc}} \frac{l_\infty c_{C,\infty}^4}{u_\infty}.$$

A different choice of  $f_\infty$  than in (9) would result in an additional factor in the last term on the left–hand side of (10).

The derivation of the equation for the dimensionless PSD proceeds in the same manner as for the other equations. One obtains from (4)

$$\frac{\partial f}{\partial t} + \mathbf{u} \cdot \nabla f + G(c_C) \frac{l_\infty}{u_\infty d_{p,\infty}} \frac{\partial f}{\partial d_p} = 0 \text{ in } (0, T] \times \Omega \times (d_{p,\text{min}}, 1) \quad (11)$$

with

$$G(c_C) = k_G c_{C,\infty} \left(c_C - \frac{c_{C,\infty}^{\text{sat}}}{c_{C,\infty}}\right).$$

Altogether, the coupled system of equations (6), (7), (8) for  $c_A$ , (8) for  $c_B$ , (10) and (11) has to be solved.

### 3 The numerical approaches for solving the population balance system

This section describes in detail the methods which were studied for solving the coupled system (6), (7), (8) for  $c_A$ , (8) for  $c_B$ , (10) and (11). The general strategy consists in first applying a temporal discretization with the same length of the time step to each equation of the system. This leads in each discrete time to a coupled system of equations which has to be linearized, discretized in space and solved iteratively.

#### 3.1 The Navier–Stokes equations

The Navier–Stokes equations (6), (7) are the first set of equations which is solved in each discrete time since they do not depend on the concentrations  $c_A, c_B, c_C$  and on the PSD  $f$ . In addition, the computed velocity field will be needed as convection field in all other equations.

Fractional–step  $\theta$ –schemes will be used for the temporal discretization of the Navier–Stokes equations. Considering the time step from  $t_{k-1}$  to  $t_k$ , with  $\Delta t_k = t_k - t_{k-1}$ , these schemes have the form

$$\begin{aligned} \mathbf{u}_k + \theta_1 \Delta t_n [-\nu \Delta \mathbf{u}_k + (\mathbf{u}_k \cdot \nabla) \mathbf{u}_k] + \Delta t_k \nabla p_k \\ = \mathbf{u}_{k-1} - \theta_2 \Delta t_n [-\nu \Delta \mathbf{u}_{k-1} + (\mathbf{u}_{k-1} \cdot \nabla) \mathbf{u}_{k-1}] \\ + \theta_3 \Delta t_n \mathbf{f}_{k-1} + \theta_4 \Delta t_n \mathbf{f}_k, \end{aligned} \quad (12)$$

$$\nabla \cdot \mathbf{u}_k = 0, \quad (13)$$

with the parameters  $\theta_1, \dots, \theta_4$  and the right–hand side  $\mathbf{f}$  of the Navier–Stokes equations. In our application is  $\mathbf{f} = \mathbf{0}$ , see (6), therefore the last two terms on the right–hand side are not present.

In the numerical studies the Crank–Nicolson scheme ( $\theta_1 = \theta_2 = \theta_3 = \theta_4 = 0.5$ ) will be used. This is an implicit, second order and A–stable scheme but it is not strongly A–stable. In numerical studies for incompressible flows, the Crank–Nicolson scheme has shown a good relation of accuracy to efficiency [15]. In particular, it was considerably more accurate than the backward Euler scheme ( $\theta_1 = \theta_4 = 1, \theta_2 = \theta_3 = 0$ ), see also [9].

Next, the system (12), (13) is linearized by a fixed point iteration: Given  $(\mathbf{u}_k^{(0)}, p_k^{(0)})$ , compute

$$\begin{aligned} \mathbf{u}_k^{(n)} + 0.5 \Delta t_n [-\nu \Delta \mathbf{u}_k^{(n)} + (\mathbf{u}_k^{(n-1)} \cdot \nabla) \mathbf{u}_k^{(n)}] + \Delta t_k \nabla p_k^{(n)} \\ = \mathbf{u}_{k-1} - 0.5 \Delta t_n [-\nu \Delta \mathbf{u}_{k-1} + (\mathbf{u}_{k-1} \cdot \nabla) \mathbf{u}_{k-1}] \end{aligned} \quad (14)$$

$$\nabla \cdot \mathbf{u}_k^{(n)} = 0, \quad n = 1, 2, \dots \quad (15)$$

The linear system (14), (15) (Oseen equations) is discretized in space with an inf–sup stable finite element method. We will use the  $Q_2$  finite element for the velocity and the  $P_1^{\text{disc}}$  (discontinuous linears) finite element for the pressure. This pair of finite element spaces has been proven to be among the best performing ones for discretizing the incompressible Navier–Stokes equations [6, 9, 10, 13]. Since laminar flows will be considered in the numerical studies, a stabilization of the spatial discretization of the Navier–Stokes equations, [1], or the application of a turbulence model, [26], is not necessary. After having solved the Navier–Stokes equations in the discrete time  $t_k$ , the velocity field is computed which is used in the convective terms of the other equations of the coupled systems.

### 3.2 The equations for the chemical reaction

The equations (8) and (10) for the chemical reaction are described by the same type of scalar convection–diffusion–reaction equation. We will apply a similar strategy for their discretization.

For simplicity of presentation, we will describe the discretization for a linear convection–diffusion–reaction equation of the form

$$\begin{aligned} \frac{\partial c}{\partial t} - \varepsilon \Delta c + \mathbf{u} \cdot \nabla c + rc &= f & \text{in } (0, T] \times \Omega, \\ c &= c_D & \text{in } (0, T] \times \partial\Omega_D, \\ \varepsilon \nabla c \cdot \mathbf{n} &= 0 & \text{in } (0, T] \times \partial\Omega_N, \\ c(0, \cdot) &= c_0 & \text{in } \Omega, \end{aligned} \tag{16}$$

where  $\partial\Omega_D$  is the Dirichlet boundary,  $\partial\Omega_N$  the Neumann boundary,  $c_D$  the prescribed boundary values of  $c$  and  $c_0$  the initial concentration. The convection field and the reaction coefficient are considered to be time–dependent. Like for the Navier–Stokes equations, we will apply a Crank–Nicolson scheme for the temporal discretization of (16)

$$\begin{aligned} &c_k + 0.5\Delta t_k(-\varepsilon\Delta c_k + \mathbf{u}_k \cdot \nabla c_k + r_k c_k) \\ &= c_{k-1} - 0.5\Delta t_k(-\varepsilon\Delta c_{k-1} + \mathbf{u}_{k-1} \cdot \nabla c_{k-1} + r_{k-1} c_{k-1}) \\ &\quad + 0.5\Delta t_k f_{k-1} + 0.5\Delta t_k f_k. \end{aligned} \tag{17}$$

In the next step, (17) is transformed into a variational formulation. Let  $V_D$  be the set of all functions from the Sobolev space  $H^1(\Omega)$  which satisfy the Dirichlet boundary conditions on  $\partial\Omega_D$  and  $V_0$  the space of all functions from  $H^1(\Omega)$  which vanish on  $\partial\Omega_D$ . A variational formulation of (17) reads

as follows: Find  $c_k \in V_D$  such that

$$\begin{aligned} & (c_k, v) + 0.5\Delta t_k \left[ (\varepsilon \nabla c_k, \nabla v) + (\mathbf{u}_k \cdot \nabla c_k + r_k c_k, v) \right] \\ &= (c_{k-1}, v) - 0.5\Delta t_k \left[ (\varepsilon \nabla c_{k-1}, \nabla v) + (\mathbf{u}_{k-1} \cdot \nabla c_{k-1} + r_{k-1} c_{k-1}, v) \right] \\ & \quad + 0.5\Delta t_k (f_{k-1}, v) + 0.5\Delta t_k (f_k, v) \end{aligned} \quad (18)$$

for all  $v \in V_0$ .

The Galerkin finite element formulation of (18) is obtained by replacing the infinite dimensional spaces  $V_D, V_0$  by finite element spaces. We will use the  $Q_1$  finite element. However, it is known that this discretization is not stable for convection– or reaction–dominated problems, [28]. In the precipitation process, the equations are strongly convection– and reaction–dominated. The use of the Galerkin finite element method would lead to huge spurious oscillations in the computed solutions which make them useless. The remedy consists in the application of a stabilized discretization.

Two approaches for stabilizing the reaction– and convection–dominated equations describing the chemical reaction were already studied in [16]. The first approach was the streamline–upwind Petrov–Galerkin (SUPG) method from [8]. This is currently the most popular way for stabilizing such equations in the framework of finite element methods. The use of this method resulted in considerable spurious oscillations in the computed concentrations. The size of these oscillations led to difficulties in obtaining stable simulations. We had to apply some cut–off techniques for negative and positive oscillations. But there were even cases where, despite the cut–off, these oscillations caused a blow–up of the simulations, see [16] for details. The second approach for stabilization considered in [16] was a Samarskij upwind scheme [28, 32]. This method led to a large smearing of the concentrations. This smearing caused the growth of unphysically large particles and finally a blow–up of the simulation.

Inspired by the bad experiences with the SUPG method and the upwind method, comprehensive numerical studies of stabilized finite element methods for scalar time–dependent convection–diffusion–reaction equations were performed in [17, 18]. These studies included besides the SUPG method a number of Spurious Oscillations at Layers Diminishing (SOLD) schemes [11, 12], a local projection stabilization (LPS) scheme [25] and two Finite–Element–Method Flux–Corrected–Transport (FEM–FCT) schemes [21, 22, 23]. All studies in [17, 18] led to the consistent conclusion that the FEM–FCT schemes are far better than the other approaches. In particular, a linear FEM–FCT scheme from [21] showed a very good relation of accuracy and efficiency. This scheme will be used for the simulation of the equations de-

scribing the chemical reactions. For completeness of presentation, a short description of this scheme will be provided.

FEM–FCT schemes have been developed for transport equations, i.e. equations of the form (16) with  $\varepsilon = r = f = 0$ . An extension to convection–diffusion–reaction equations can be found in [18]. These schemes work on the algebraic level and they modify the system matrix and the right–hand side vector.

Starting point of the linear FEM–FCT scheme used in the simulations presented in Section 4 is the Crank–Nicolson scheme and the Galerkin finite element method, which can be written in the matrix–vector form

$$(M_C + 0.5\Delta t_k A)\underline{u}_k = (M_C - 0.5\Delta t_k A)\underline{u}_{k-1} + 0.5\Delta t_k \underline{f}_{k-1} + 0.5\Delta t_k \underline{f}_k, \quad (19)$$

where  $M_C$  is the consistent mass matrix. The matrix  $A$  is the sum of diffusion, convection and reaction. The notations  $\underline{u}_k, \underline{f}_k$  etc. stand for the vectors of the unknown coefficients of the finite element method. It is well known that the solution of (19) generally shows huge spurious oscillations.

FEM–FCT schemes start by defining the matrices

$$\begin{aligned} L &= A + D, \\ D &= (d_{ij}), \quad d_{ij} = -\max\{0, a_{ij}, a_{ji}\} = \min\{0, -a_{ij}, -a_{ji}\} \text{ for } i \neq j, \\ d_{ii} &= -\sum_{j=1, j \neq i}^N d_{ij}, \end{aligned} \quad (20)$$

$$M_L = \text{diag}(m_i), \quad m_i = \sum_{j=1}^N m_{ij}, \quad (21)$$

where  $N$  is the number of degrees of freedom. The row and column sums of  $D$  are zero. The matrix  $L$  does not possess positive off–diagonal entries and the diagonal matrix  $M_L$  is called lumped mass matrix. Instead of (19), the equation

$$(M_L + 0.5\Delta t_k L)\underline{u}_k = (M_L - 0.5\Delta t_k L)\underline{u}_{k-1} + 0.5\Delta t_k \underline{f}_{k-1} + 0.5\Delta t_k \underline{f}_k \quad (22)$$

is considered. This is the algebraic representation of a stable low order scheme. The solution of (22) does not show spurious oscillations, however layers will be smeared because the operator on the left–hand side is too diffusive.

In the next step, a FEM–FCT scheme modifies the right–hand side of (22) such that the diffusion is removed where it is not needed and spurious oscillations are still suppressed

$$\begin{aligned} (M_L + 0.5\Delta t_k L)\underline{u}_k &= (M_L - 0.5\Delta t_k L)\underline{u}_{k-1} + 0.5\Delta t_k \underline{f}_{k-1} + 0.5\Delta t_k \underline{f}_k \\ &\quad + \underline{f}^*(\underline{u}_k, \underline{u}_{k-1}). \end{aligned} \quad (23)$$

The ansatz for the vector  $\underline{f}^*(\underline{u}_k, \underline{u}_{k-1})$  uses the residual vector of (22) and (19)

$$\begin{aligned}\underline{r} &= \left( M_L + 0.5\Delta t_k L - (M_C + 0.5\Delta t_k A) \right) \underline{u}_k \\ &\quad - \left( M_L - 0.5\Delta t_k L - (M_C - 0.5\Delta t_k A) \right) \underline{u}_{k-1} \\ &= (M_L - M_C)(\underline{u}_k - \underline{u}_{k-1}) + \Delta t_k D(0.5\underline{u}_k + 0.5\underline{u}_{k-1}).\end{aligned}$$

The residual vector has to be weighted appropriately. To this end, it is decomposed into fluxes  $r_{ij}$ ,  $i, j = 1, \dots, N$ , in the following way

$$\begin{aligned}\underline{r}_i = \sum_{j=1}^N r_{ij} &= \sum_{j=1}^N \left[ m_{ij}(\underline{u}_{k,i} - \underline{u}_{k,j}) - m_{ij}(\underline{u}_{k-1,i} - \underline{u}_{k-1,j}) \right. \\ &\quad \left. - \Delta t_k 0.5 d_{ij}(\underline{u}_{k,i} - \underline{u}_{k,j}) - \Delta t_k 0.5 d_{ij}(\underline{u}_{k-1,i} - \underline{u}_{k-1,j}) \right] \quad (24)\end{aligned}$$

$i = 1, \dots, N$ . The fluxes can be written in the form

$$\begin{aligned}r_{ij} &= m_{ij}(\underline{u}_{k,i} - \underline{u}_{k-1,i}) - m_{ij}(\underline{u}_{k,j} - \underline{u}_{k-1,j}) \\ &\quad - 0.5\Delta t_k d_{ij}(\underline{u}_{k,i} + \underline{u}_{k-1,i}) + 0.5\Delta t_k d_{ij}(\underline{u}_{k,j} + \underline{u}_{k-1,j}). \quad (25)\end{aligned}$$

The ansatz for the correction vector is now given by

$$\underline{f}_i^*(\underline{u}_k, \underline{u}_{k-1}) = \sum_{j=1}^N \alpha_{ij} r_{ij}, \quad i = 1, \dots, N,$$

with the weights  $\alpha_{ij} \in [0, 1]$ . In the methods proposed in [22, 23],  $\underline{f}^*(\underline{u}_k, \underline{u}_{k-1})$  is a nonlinear term.

A linear FEM–FCT scheme was presented recently in [21]. The idea of this scheme consists in replacing  $\underline{u}_k$  in (25) by an approximation which can be computed with an explicit scheme. To this end, define the intermediate value

$$\underline{u}_{k-1/2} := \frac{\underline{u}_k + \underline{u}_{k-1}}{2}.$$

Inserting this value into (25) gives

$$\begin{aligned}r_{ij} &= 2m_{ij}(\underline{u}_{k-1/2,i} - \underline{u}_{k-1,i}) - 2m_{ij}(\underline{u}_{k-1/2,j} - \underline{u}_{k-1,j}) \\ &\quad - \Delta t_k d_{ij}(\underline{u}_{k-1/2,i} - \underline{u}_{k-1/2,j}). \quad (26)\end{aligned}$$

An approximation of  $\underline{u}_{k-1/2}$  can be obtained by using the forward Euler scheme in the discrete time  $t_{k-1}$  with the time step  $\Delta t_k/2$ , leading to

$$\tilde{\underline{u}} = \underline{u}_{k-1} - \frac{\Delta t_k}{2} M_L^{-1} (L \underline{u}_{k-1} - \underline{f}_{k-1}). \quad (27)$$

Inserting this approximation into (26) gives the fluxes in the linear FEM–FCT scheme

$$r_{ij} = \Delta t_k [m_{ij}(\underline{v}_{k-1/2,i} - \underline{v}_{k-1/2,j}) - d_{ij}(\tilde{u}_i - \tilde{u}_j)]$$

with

$$\underline{v}_{k-1/2,i} = \left( M_L^{-1}(\underline{f}_{k-1} - L\underline{u}_{k-1}) \right)_i, \quad \tilde{u}_i = \underline{u}_{k-1,i} + \frac{\Delta t_k}{2} \underline{v}_{k-1/2,i}.$$

For computing the weights, Zalesak’s algorithm [35] is used. We refer to [18, 22] for presentations of this algorithm. Some details on the implementation of FEM–FCT schemes can be found also in [18].

Since the auxiliary solution  $\tilde{u}$  in (27) is computed with an explicit scheme, the stability of this step requires the fulfillment of a CFL condition. This condition is [21, 22]

$$\Delta t_k < 2 \min_i \frac{m_i}{l_{ii}}. \quad (28)$$

It was fulfilled in all simulations presented in Section 4.

The coupled nonlinear system (8) for the concentrations  $c_A$  and  $c_B$  in  $t_k$  is solved iteratively with a fixed point iteration, where one iteration consists of two sub–steps:

1. solve the FEM–FCT discretization of (8) for  $c_{A,k}$  with the currently available approximation of  $c_{B,k}$ ,
2. solve the FEM–FCT discretization of (8) for  $c_{B,k}$  with the approximation of  $c_{A,k}$  computed in the first sub–step.

In the first iteration in the discrete time  $t_k$ , the currently available approximation of  $c_{B,k}$  is  $c_{B,k-1}$ . Note that in this iterative procedure, only the reaction coefficient  $r_k$  is updated. In particular, the right–hand side of (18) does not change. The iteration is stopped if the residual of the coupled system is sufficiently small, whereas this criterion is checked only after performing both sub–steps of the fixed point iteration.

After having computed the concentrations  $c_A$  and  $c_B$ , the next step in our solution algorithm consists in computing  $c_C$  by solving (10). In order to facilitate the computation of  $c_C$ , the last two terms on the left–hand side of (10) are treated explicitly in time with respect to  $c_C$ , leading after the

temporal discretization to the linear equation

$$\begin{aligned}
& c_{C,k} + 0.5\Delta t_k \left( -\frac{D_C}{u_\infty l_\infty} \Delta c_{C,k} + \mathbf{u}_k \cdot \nabla c_{C,k} \right) \\
&= c_{C,k-1} + 0.5\Delta t_k \left( -\frac{D_C}{u_\infty l_\infty} \Delta c_{C,k-1} + \mathbf{u}_{k-1} \cdot \nabla c_{C,k-1} \right) \\
&+ 0.5\Delta t_k \left[ \Lambda_{\text{chem}} \left( c_{A,k-1} c_{B,k-1} + c_{A,k} c_{B,k} \right) \right. \\
&- \Lambda_{\text{nuc}} \left( \max \{0, (c_{C,k-2} - 1)^5\} + \max \{0, (c_{C,k-1} - 1)^5\} \right) \\
&+ 0.5\Delta t_k \left( \Lambda_{\text{chem}} c_{A,k} c_{B,k} - \Lambda_{\text{nuc}} \max \{0, (c_{C,k-1} - 1)^5\} \right. \\
&- \left. \left( c_{C,k-2} - \frac{c_{C,\infty}^{\text{sat}}}{c_{C,\infty}} \right) \int_{d_{p,\min}}^1 d_p^2 f_{k-2} d(d_p) \right. \\
&- \left. \left. \left( c_{C,k-1} - \frac{c_{C,\infty}^{\text{sat}}}{c_{C,\infty}} \right) \int_{d_{p,\min}}^1 d_p^2 f_{k-1} d(d_p) \right] \right]. \tag{29}
\end{aligned}$$

This is a linear convection–diffusion–reaction equation in  $t_k$  (the reactive term originates from the discretization in time) which has to be solved. For the spatial discretization and stabilization of this equation as well the linear FEM–FCT scheme will be applied. After having solved (29), all concentrations at time  $t_k$  are computed.

The transport equation (11) modeling the PSD is given in a higher dimensional domain than the other equations. Thus, the solution of (11) can be expected to be much more expensive than the solution of the rest of the equations. The main goal of this paper consists in studying different approaches for discretizing (11) and exploring the impact of using expensive, higher order discretizations and inexpensive, low order methods on the accuracy and the computing times.

The first approach which will be studied is the linear FEM–FCT scheme described above. Since FEM–FCT schemes were originally designed for transport equations, they can be readily applied for solving (11). After having assembled the matrices and the arrays arising in the  $Q_1$  Galerkin finite element discretization of (11), the same procedure as given above was used to apply the linear FEM–FCT scheme to these matrices and arrays. With this scheme, a rather accurate solution can be expected. However, this scheme is quite expensive for several reasons. First, assembling finite element matrices in higher dimensions requires quadrature rules with sufficiently many quadrature points. The application of such rules in three and higher dimen-

sions is quite time-consuming [10]. Second, the flux-correction procedure becomes more expensive for an increasing number of degrees of freedom and for an increasing connectivity of the matrix entries. Both situations arise in higher dimensions. And last, a linear system of equations has to be solved in each discrete time. For the reason of efficiency, it is worthwhile to consider less expensive (and generally less accurate) approaches as alternatives and to compare the computed results.

Two less expensive approaches will be studied for the discretization of the transport equation for the PSD (11), a forward and a backward Euler finite difference upwind method, [24]. In the forward Euler scheme, the already computed fields  $\mathbf{u}_k^h$  and  $c_{C,k}^h$  will be used, leading to

$$f_k^h = f_{k-1}^h - \Delta t_k \left( \mathbf{u}_k^h \cdot \nabla f_{k-1}^h + \frac{k_G c_{C,\infty} l_\infty}{u_\infty d_{p,\infty}} \left( c_{C,k}^h - \frac{c_{C,\infty}^{\text{sat}}}{c_{C,\infty}} \right) \frac{\partial f_{k-1}^h}{\partial d_p} \right). \quad (30)$$

The convective terms on the right-hand side are discretized by an upwind scheme. Consider, for instance, the node  $(\mathbf{x}, d_{p,i})$ . Then, the upwinding scheme approximates the convective term with respect to the internal coordinate in  $(\mathbf{x}, d_{p,i})$  by

$$\left( G_k^h \frac{\partial f_{k-1}^h}{\partial d_p} \right) (\mathbf{x}, d_{p,i}) \approx \begin{cases} G_k^h(\mathbf{x}) \frac{f_{k-1}^h(\mathbf{x}, d_{p,i}) - f_{k-1}^h(\mathbf{x}, d_{p,i-1})}{d_{p,i} - d_{p,i-1}} & \text{if } G_k^h(\mathbf{x}) \geq 0, \\ G_k^h(\mathbf{x}) \frac{f_{k-1}^h(\mathbf{x}, d_{p,i+1}) - f_{k-1}^h(\mathbf{x}, d_{p,i})}{d_{p,i+1} - d_{p,i}} & \text{if } G_k^h(\mathbf{x}) < 0, \end{cases} \quad (31)$$

where

$$G_k^h(\mathbf{x}) = \frac{k_G c_{C,\infty} l_\infty}{u_\infty d_{p,\infty}} \left( c_{C,k}^h(\mathbf{x}) - \frac{c_{C,\infty}^{\text{sat}}}{c_{C,\infty}} \right),$$

and  $(\mathbf{x}, d_{p,i-1})$ ,  $(\mathbf{x}, d_{p,i+1})$  are the neighbor nodes of  $(\mathbf{x}, d_{p,i})$  with respect to this coordinate. It can be immediately seen from (30) that the computation of  $f_k^h$  using the forward Euler upwind finite difference (FWE-UPW-FDM) approach does not require the solution of a linear system of equations.

The backward Euler temporal discretization of (11) is given by

$$f_k^h + \Delta t_k \left( \mathbf{u}_k^h \cdot \nabla f_k^h + \frac{k_G c_{C,\infty} l_\infty}{u_\infty d_{p,\infty}} \left( c_{C,k}^h - \frac{c_{C,\infty}^{\text{sat}}}{c_{C,\infty}} \right) \frac{\partial f_k^h}{\partial d_p} \right) = f_{k-1}^h. \quad (32)$$

The discretization of the convective terms in (32) is done with an upwind approach similar to (31), replacing  $f_{k-1}^h$  by  $f_k^h$  and leading to off-diagonal entries in the system matrix. The backward Euler scheme requires the solution of a linear system of equations in each discrete time. This approach will be called BWE-UPW-FDM in the following.

The numerical tests in Section 4 study the flow in a cavity. This squared flow domain is especially suitable for the application of finite difference methods. The FEM–FCT method for solving the PSD equation was applied with the  $Q_1$  finite element on an anisotropic hexahedral grid. The matrix  $M_L$  in (23) was computed in a preprocessing step since this matrix does not change during the simulation. In each step of the simulation, the matrix  $A$  has to be assembled, from which  $L$  in (23) is derived. The term with the highest polynomial degree in the FEM–FCT method applied to the PSD equation is the transport term in spatial direction. The finite element velocity is a two-dimensional  $Q_2$  function (polynomial of degree 2 in  $x$  and degree 2 in  $y$ ) and the spatial gradient of the finite element PSD function is a bilinear function. Hence, the product is a polynomial of degree 3 in both of the spatial variables. We applied a Gaussian quadrature rule with two quadrature points in each direction (eight quadrature points in the three-dimensional mesh cell) which is exact for polynomials of degree 3 in each coordinate. The numerical studies will show that this approach is rather expensive in comparison with BWE–UPW–FDM (32). In addition, the algorithm for computing the flux limiters has to be performed at each discrete time, which is also time-consuming. The memory requirements are also quite different in the three approaches for discretizing the PSD equation. Whereas in the FWE–UPW–FDM the additional memory is negligible, one has to store a higher-dimensional system matrix in the implicit methods. The FEM–FCT matrix has a stronger connectivity, i.e. more matrix entries, than the BWE–UPW–FDM matrix. To speed up the assembling of the matrix in the FEM–FCT method, we stored at the initial time information of some search operations. The speed up was considerable but also the arising memory overhead increased notably.

## 4 Numerical simulations

### 4.1 Setup of the simulations

The population balance system was simulated in the cavity  $\Omega = (0, 1)^2$ , see Figure 1. The size of the inlets is  $1/32$  and the size of the outlet  $1/16$ . The center of the outlet is situated at  $(0.5, 0)$ . The center of the left inlet is situated at  $(0, 31/64)$  and the center of the right one at  $(1, 31/64)$ . A configuration of this type is sometimes called T-mixer. Different positions of the inlets have been studied in [16].

For the Navier–Stokes equations (6), (7), parabolic inflow profiles with an integral mean value of 1 (maximal value of 1.5) were applied. Outflow boundary conditions were used at the outlet. The concentrations of the reactants A at

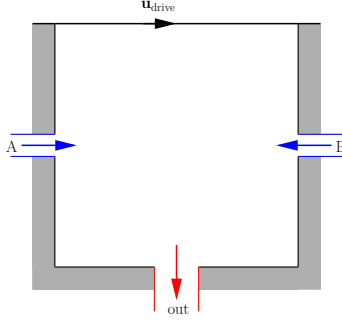


Figure 1: Cavity with inlets and outlets.

the left inlet and B at the right inlet were set to 1 for all times

$$\begin{aligned} c_A &= 1 && \text{on } [0, T] \times [0] \times [15/32, 1/2], \\ c_B &= 1 && \text{on } [0, T] \times [1] \times [15/32, 1/2]. \end{aligned}$$

Neumann boundary conditions were used on all other parts of the boundary. For the substance  $C$ , Neumann boundary conditions were applied on the whole boundary. The boundary condition of the PSD with respect to the internal coordinate was

$$\begin{aligned} f(t, x_1, x_2, d_{p,\min}) &= \frac{B_{\text{nuc}}(c_C)}{f_\infty G(c_C)} && \text{if } G(c_C(t, x_1, x_2)) > 0, \\ f(t, x_1, x_2, d_{p,\min}) &= 0 && \text{if } G(c_C(t, x_1, x_2)) = 0, \\ f(t, x_1, x_2, d_{p,\max}) &= 0 && \text{if } G(c_C(t, x_1, x_2)) < 0, \end{aligned}$$

with  $B_{\text{nuc}}(c_C) = k_{\text{nuc}} c_{C,\infty}^5 \max\{0, (c_C - 1)^5\}$ . With respect to the spatial coordinates, the PSD was set to be zero at the closure of the fluid flow inlets (see [28])

$$\begin{aligned} f(t, x_1, x_2, d_p) &= 0 && \text{on } [0, T] \times [0] \times [15/32, 1/2] \times (d_{p,\min}, d_{p,\max}], \\ f(t, x_1, x_2, d_p) &= 0 && \text{on } [0, T] \times [1] \times [15/32, 1/2] \times (d_{p,\min}, d_{p,\max}]. \end{aligned}$$

Besides the opposite inflows, the mixing of the reactants A and B was stimulated by the movement of the upper wall with the velocity  $\mathbf{u}_{\text{drive}} = (u_{1,\text{drive}}/u_\infty, 0)^T$ . The values  $u_{1,\text{drive}} = 10^{-3} \text{ m/s}$  and  $u_\infty \in \{10^{-3}, 10^{-2}\} \text{ m/s}$  were used in the simulations presented below.

The initial velocity fields were fully developed flows, computed in a preprocessing step. Initially, the concentrations were zero in  $\Omega$ . The inflow of the reactants started at  $t = 0$ . There were no particles in the flow at  $t = 0$  such that the initial condition of the PSD was also zero.

In the numerical simulations, the calcium carbonate precipitation



has been considered. The physical and chemical parameters of this process are given by [2, 4, 33, 34]:

- $\nu = 10^{-6} \text{ m}^2/\text{s}$
- $\rho = 1 \text{ kg}/\text{m}^3$
- $k_G = 10^{-7} \text{ m}^4/(\text{kmol s})$
- $k_{\text{nuc}} = 10^{24} (1/(\text{m}^3 \text{ s}))/(\text{kmol}/\text{m}^3)^5$
- $k_R = 10 \text{ m}^3/(\text{kmol s})$
- $c_{C,\infty}^{\text{sat}} = 1.37 \cdot 10^{-4} \text{ kmol}/\text{m}^3$
- $C_2 = 7.2 \cdot 10^{-9} \text{ m}$
- $C_G = 45.98 \text{ kmol}/\text{m}^3$
- $C_{\text{nuc}} = 15.33 \text{ kmol}/\text{m}^3$
- $D_A = D_B = D_C = 1.5 \cdot 10^{-9} \text{ m}^2/\text{s}$
- $\tilde{d}_{p,0} = 10^{-9} \text{ m}$
- $\tilde{d}_{p,\text{max}} = 10^{-4} \text{ m}$

The following reference quantities have been used to derive the dimensionless equations:

- $l_\infty = 1 \text{ m}$
- $u_\infty = 10^{-3} \text{ m}/\text{s}$  or  $u_\infty = 10^{-2} \text{ m}/\text{s}$
- $t_\infty = 10^3 \text{ s}$  for  $u_\infty = 10^{-3} \text{ m}/\text{s}$  or  $t_\infty = 10^2 \text{ s}$  for  $u_\infty = 10^{-2} \text{ m}/\text{s}$ ,
- $c_\infty = 1 \text{ kmol}/\text{m}^3$
- $c_{C,\infty} = 0.183502 \text{ kmol}/\text{m}^3$
- $d_{p,\infty} = 10^{-4} \text{ m}$
- $f_\infty = 2.17486 \cdot 10^{14} \text{ 1}/\text{m}^4$  for  $u_\infty = 10^{-3} \text{ m}/\text{s}$ ,  $f_\infty = 2.17486 \cdot 10^{15} \text{ 1}/\text{m}^4$  for  $u_\infty = 10^{-2} \text{ m}/\text{s}$ .

The choice of  $\tilde{d}_{p,\text{max}}$  is based on the experiences from [16]. The Reynolds number of the flow with  $u_\infty = 10^{-3}$  is  $Re = 1000$  and the flow with  $u_\infty = 10^{-2}$  has  $Re = 10000$ . The reactive term in (8) has a large factor:  $k_R l_\infty c_\infty / u_\infty$ . Considering (8) for one of the reactants, the local Damköhler number was of order  $10^4$  for  $u_\infty = 10^{-3}$  and of order  $10^3$  for  $u_\infty = 10^{-2}$  in regions where the concentration of the other reactant was close to one.

The time stepping schemes were applied with equidistant time steps. The velocity field and the concentrations were computed on grids consisting of  $64 \times 64$  squares. Information on the numbers of degrees of freedom are provided in Table 1. With respect to the internal coordinate, we used grids with  $L \in \{32, 48, 64\}$  layers. The numerical studies of [16] showed that in particular small particles will appear such that the grid for the PSD has to

be refined towards  $d_{p,\min}$ . For this reason, we used anisotropic grids on which the grid points were distributed accordingly to the formula

$$d_{p,i} = 1 + (1 - d_{p,\min}) \frac{\tanh(2.75(i/L - 1))}{\tanh(2.75)}, \quad i = 0, \dots, L.$$

The numbers of degrees of freedom on these grids are given in Table 1. For all considered numbers of layers, the PSD equation is by far the largest individual equation in the coupled population balance system.

Table 1: Information on the number of degrees of freedom.

function	d.o.f.
velocity	33 282
pressure	12 288
each concentration	4 225
PSD with $L = 32$	139 425
PSD with $L = 48$	207 025
PSD with $L = 64$	274 625

Due to solving some equations approximately by iterative schemes, small negative concentrations and PSD values can occur. They were cut off for the reason of the stability of the simulations.

The linearized Navier–Stokes equations (14), (15) were solved by a flexible GMRES method [29] with a coupled multigrid preconditioner [10]. The linearized equations for the chemical reaction were solved with the direct solver UMFPACK, [3]. For the linear equations in 3D arising in the backward Euler discretization and the FEM–FCT method, we used as solver the GMRES method with an SSOR preconditioner. We could observe that in general only very few iterations were necessary to solve the PSD equation with this approach. The computations were performed with the code MoonMD [14]. In the evaluation of the process, the PSD at the center of the outflow  $(0.5, 0)$  was considered. For the representation of the PSD in this point, the volume fraction  $q_3$  defined by

$$q_3(\tilde{t}, \tilde{d}_p) := \frac{\tilde{d}_p^3 \tilde{f}(\tilde{t}, 0.5l_\infty, 0, \tilde{d}_p)}{\int_{\tilde{d}_{p,0}}^{\tilde{d}_{p,\max}} \tilde{d}_p^3 \tilde{f}(\tilde{t}, 0.5l_\infty, 0, \tilde{d}_p) d(\tilde{d}_p)}$$

was used. The cumulative volume fraction is given by

$$Q_3(\tilde{t}, \tilde{d}_p) := \int_{\tilde{d}_{p,0}}^{\tilde{d}} q_3(\tilde{t}, \tilde{d}_p) d(\tilde{d}_p).$$

With  $Q_3(\tilde{t}, \tilde{d}_p)$ , the median of the volume fraction  $\tilde{d}_{p,50}(\tilde{t})$  is defined to be the particle size for which  $Q_3(\tilde{t}, \tilde{d}_p)$  takes the value 0.5:

$$\tilde{d}_{p,50}(\tilde{t}) := \left\{ \tilde{d}_p : Q_3(\tilde{t}, \tilde{d}_p) = 0.5 \right\}. \quad (33)$$

The value  $\tilde{d}_{p,50}(\tilde{t})$  is a kind of expectation of the volume fraction.

All simulations were performed in the dimensionless time interval  $[0, 200]$  with precomputed fully developed velocity fields as initial condition for the Navier–Stokes equations. The velocity fields were obtained by solving the Navier–Stokes equations in a time interval of 100 (non–dimensionalized) seconds, starting with a zero initial condition. Besides the median of the volume fraction at the center of the outlet, we consider time–averages of this quantity. Time–averaged values are often of great importance in applications. The time–averages presented below were computed in the interval  $[100, 200]$ .

## 4.2 Studies with $u_\infty = 10^{-3}$

The case  $u_\infty = 10^{-3}$  leads to a population balance system where the structures of the flow field and of the concentrations showed only small changes in time. Typical forms of the flow field and the distributions of the concentrations are presented in Figure 2. A typical evolution of the median of the volume fraction is shown in Figure 3. The structure of the flow field is governed by the dominating influence of the movement of the upper wall. It can be seen that the precipitation process starts at around 10 000 seconds and at the beginning of the precipitation process some peaks occur in  $\tilde{d}_{p,50}(\tilde{t})$ . But after a while, a periodic behavior of  $\tilde{d}_{p,50}(\tilde{t})$  starts where the length of the period and the amplitude of the oscillations depend on the scheme used for solving the PSD equation.

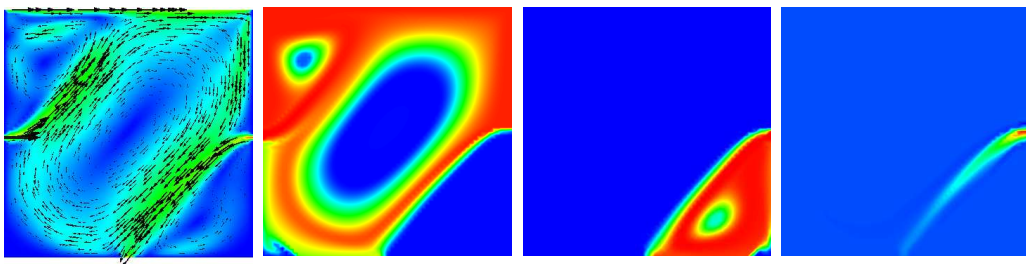


Figure 2: Typical simulation for the case  $u_\infty = 10^{-3}$ ; here FEM–FCT with  $\Delta t = 0.00125$ , ( $\Delta \tilde{t} = 1.25$  s),  $L = 64$  at  $\tilde{t} = 100\,000$  s; left to right: velocity, concentration of  $CaCl_2$ ,  $Na_2CO_3$  and dissolved  $CaCO_3$ .

The averaged medians of the volume fraction are presented in Table 2. It can be seen that the time step of the simulations has a great influence on the results. The results for  $\Delta t = 0.005$  ( $\Delta \tilde{t} = 5$  s) are rather different to the finer time steps, in particular for the first order Euler schemes FWE–UPW–FDM and BWE–UPW–FDM. This indicates that the results are too inaccurate and the time step  $\Delta t = 0.005$  is too large. Refining the internal coordinate leads also to considerable changes in the time–averaged medians of the volume fraction. With respect to this quantity, all schemes for discretizing the PSD give results of the same order of magnitude for sufficiently small time steps. A convergence of the results cannot yet be observed, the asymptotic limit does not seem to be reached.

Table 2: Studies with  $u_\infty = 10^{-3}$ : averaged median of the volume fraction.

$L$	disc. PSD equ.	$\Delta t = 0.005$	$\Delta t = 0.0025$	$\Delta t = 0.00125$
		$\Delta \tilde{t} = 5$ s	$\Delta \tilde{t} = 2.5$ s	$\Delta \tilde{t} = 1.25$ s
32	FWE–UPW–FDM	4.096e-6	6.855e-6	6.365e-6
	BWE–UPW–FDM	5.363e-6	7.061e-6	6.624e-6
	FEM–FCT	5.671e-6	5.750e-6	6.239e-6
48	FWE–UPW–FDM	3.391e-6	5.743e-6	5.296e-6
	BWE–UPW–FDM	4.446e-6	5.983e-6	5.520e-6
	FEM–FCT	4.874e-6	5.110e-6	5.563e-6
64	FWE–UPW–FDM	3.055e-6	5.235e-6	4.809e-6
	BWE–UPW–FDM	4.030e-6	5.487e-6	5.020e-6
	FEM–FCT	4.497e-6	4.793e-6	5.354e-6

Typical evolutions of the median of the volume fraction are presented in Figure 3. All schemes finally show an oscillatory behavior. The oscillations obtained with the first order Euler/upwind finite difference schemes are smaller than with the Crank–Nicolson FEM–FCT scheme. We think that the reason is that the former schemes are more diffusive.

The averaged computing times per time step are presented in Table 3. Using the FWE–UPW–FDM scheme for discretizing the PSD equation results in a negligible overhead to the simulation of the flow and the chemical reaction. The computing times for this approach are essentially the computing times for solving the flow equations and reaction equations of the population balance system. The computing times for both implicit approaches increase with the number of layers for the internal coordinate. In the BWE–UPW–FDM, the overhead comes essentially from solving the linear PSD equation. In the FEM–FCT scheme, in addition the assembling of the matrices is more expensive and the flux correction has to be computed. The implicit approaches

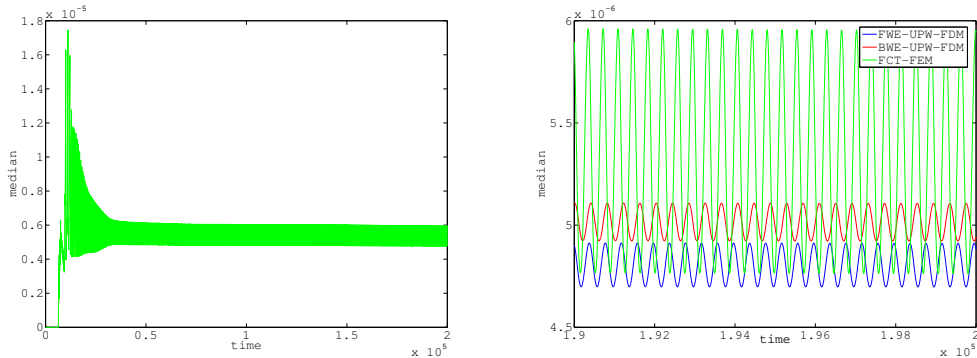


Figure 3: Typical evolution of the median of the volume fraction for the case  $u_\infty = 10^{-3}$ ; left: FEM–FCT with  $\Delta t = 0.00125$ , ( $\Delta \tilde{t} = 1.25$  s),  $L = 64$ ; right: all discretizations of the PSD equation with  $\Delta t = 0.00125$ , ( $\Delta \tilde{t} = 1.25$  s),  $L = 64$ .

give somewhat better results with respect to the median of the volume fraction for the largest time step  $\Delta t = 0.005$ . However, the differences to the results of FWE–UPW–FDM decrease for smaller time steps.

Table 3: Studies with  $u_\infty = 10^{-3}$ : averaged computing time per time step in seconds.

$L$	disc. PSD equ.	$\Delta t = 0.005$	$\Delta t = 0.0025$	$\Delta t = 0.00125$
		$\Delta \tilde{t} = 5$ s	$\Delta \tilde{t} = 2.5$ s	$\Delta \tilde{t} = 1.25$ s
32	FWE–UPW–FDM	4.55	2.89	1.25
	BWE–UPW–FDM	5.51	3.90	2.36
	FEM–FCT	6.77	5.24	3.79
48	FWE–UPW–FDM	4.53	2.97	1.25
	BWE–UPW–FDM	6.74	5.20	2.99
	FEM–FCT	7.99	6.63	5.10
64	FWE–UPW–FDM	4.67	2.92	1.24
	BWE–UPW–FDM	7.86	5.63	3.70
	FEM–FCT	10.14	8.00	6.36

In this example, all discretizations of the PSD equation gave for sufficiently small time steps qualitatively similar results. The explicit approach was by far the fastest method.

Table 4: Studies with  $u_\infty = 10^{-2}$ : averaged median of the volume fraction.

$L$	disc. of PSD equ.	$\Delta t = 0.0025$	$\Delta t = 0.00125$	$\Delta t = 0.000625$
		$\Delta \tilde{t} = 0.25 \text{ s}$	$\Delta \tilde{t} = 0.125 \text{ s}$	$\Delta \tilde{t} = 0.0625 \text{ s}$
32	FWE–UPW–FDM	1.328e-5	8.418e-6	9.032e-6
	BWE–UPW–FDM	1.368e-5	8.485e-6	9.064e-6
	FEM–FCT	3.252e-5	3.447e-5	3.344e-5
48	FWE–UPW–FDM	1.151e-5	6.919e-6	7.355e-6
	BWE–UPW–FDM	1.203e-5	6.975e-6	7.386e-6
	FEM–FCT	2.183e-5	1.528e-5	1.887e-5
64	FWE–UPW–FDM	1.125e-5	6.227e-6	6.591e-6
	BWE–UPW–FDM	1.207e-5	6.281e-6	6.621e-6
	FEM–FCT	1.916e-5	1.233e-5	1.643e-5

### 4.3 Studies with $u_\infty = 10^{-2}$

These studies consider a highly time-dependent problem with changing structures, see Figure 4 for an illustration. The influence of the movement of the upper wall is rather small and the structure of the flow field is dominated by the inflows from the opposite inlets. We had to apply some damping in the coupled multigrid preconditioner for solving the linearized and discretized Navier–Stokes equations in order to perform stable simulations for  $\Delta t = 0.000625$  ( $\Delta \tilde{t} = 0.0625 \text{ s}$ ). The time step  $\Delta t = 0.005$  ( $\Delta \tilde{t} = 0.5$ ) is too large for the application of the FEM–FCT scheme in the simulation of the chemical reaction since the CFL condition (28) is violated.

Results obtained with the different schemes for solving the population balance equation are presented in Tables 4, 5 and in Figure 5. The average particles are larger than in the simulation with  $u_\infty = 10^{-3}$ . With the irregular flow field, the average residence time of the particles seems to be longer. In addition, dissolved  $CaCO_3$  is in much more regions of the flow domain available, not only at the layer between the right inlet and the outlet.

It can be seen that the results with both Euler schemes and the upwind finite different method are very similar. In contrast to the simulations with  $u_\infty = 10^{-3}$ , the results obtained with the Crank–Nicolson FEM–FCT scheme for solving the population balance equation are dramatically different, see Figure 5. We like to emphasize that the flow field is the same in all simulations since there is no back coupling to the Navier–Stokes equations in our model. With the FEM–FCT scheme, much larger particles than with the other schemes are obtained during the start phase of the precipitation process, up to around 7 500 seconds. After this, a sudden decrease of the

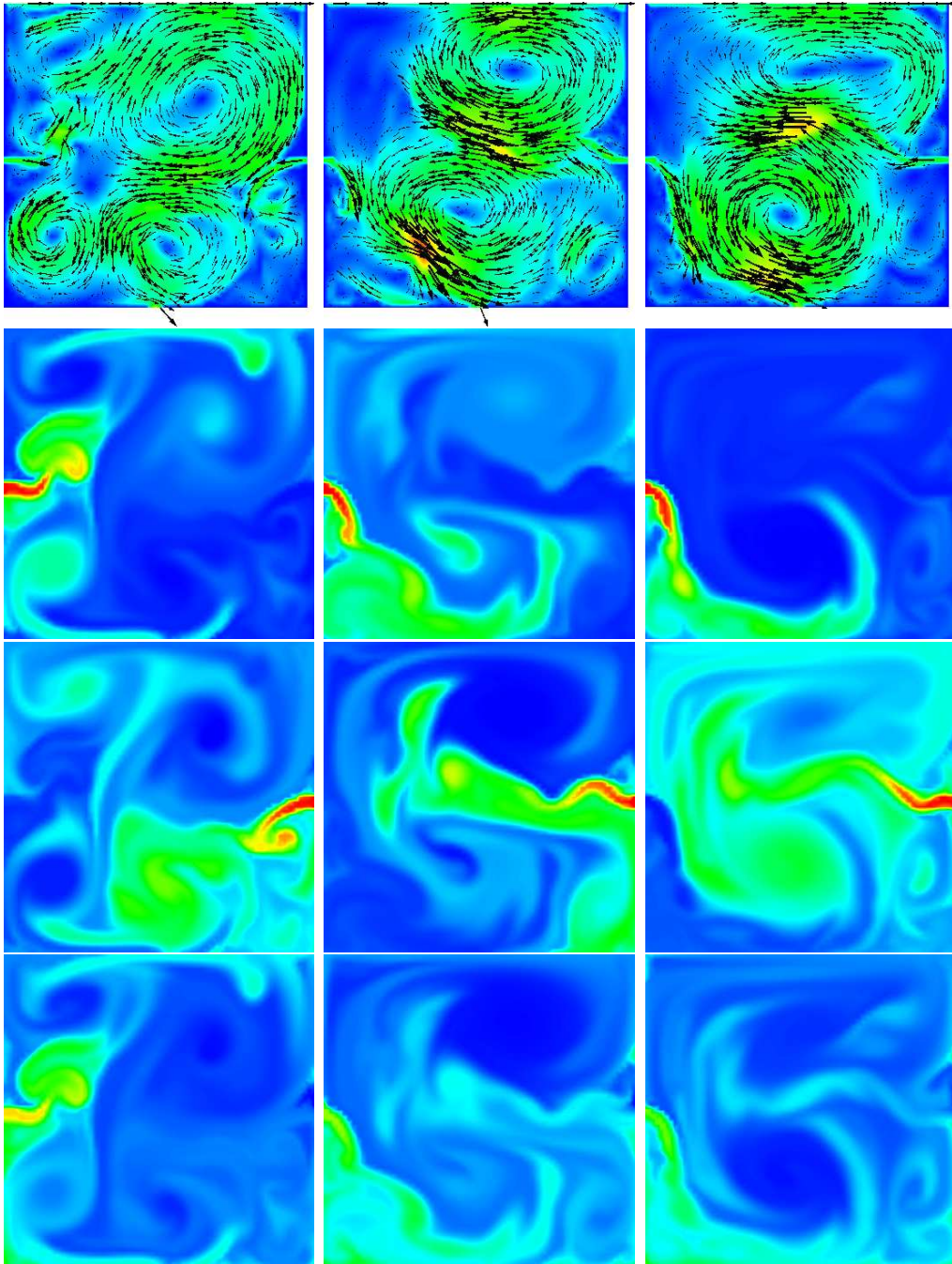


Figure 4: Simulation for the case  $u_\infty = 10^{-2}$ ; FWE-UPW-FDM with  $\Delta t = 0.00125$  ( $\Delta \tilde{t} = 0.125$ ),  $L = 64$ , at  $\tilde{t} = 10\,000, 15\,000, 20\,000$  s; top to bottom velocity, concentration of  $CaCl_2$ ,  $Na_2CO_3$  and dissolved  $CaCO_3$ .

median of the particle size can be observed. Then, the generation of comparatively large particles starts again. The curves obtained with the FEM–FCT scheme are much more oscillatory than with the other schemes. We think that the strong smearing properties of the first order Euler schemes and the first order upwind scheme are the reason for the much smoother behavior of the simulations with these schemes.

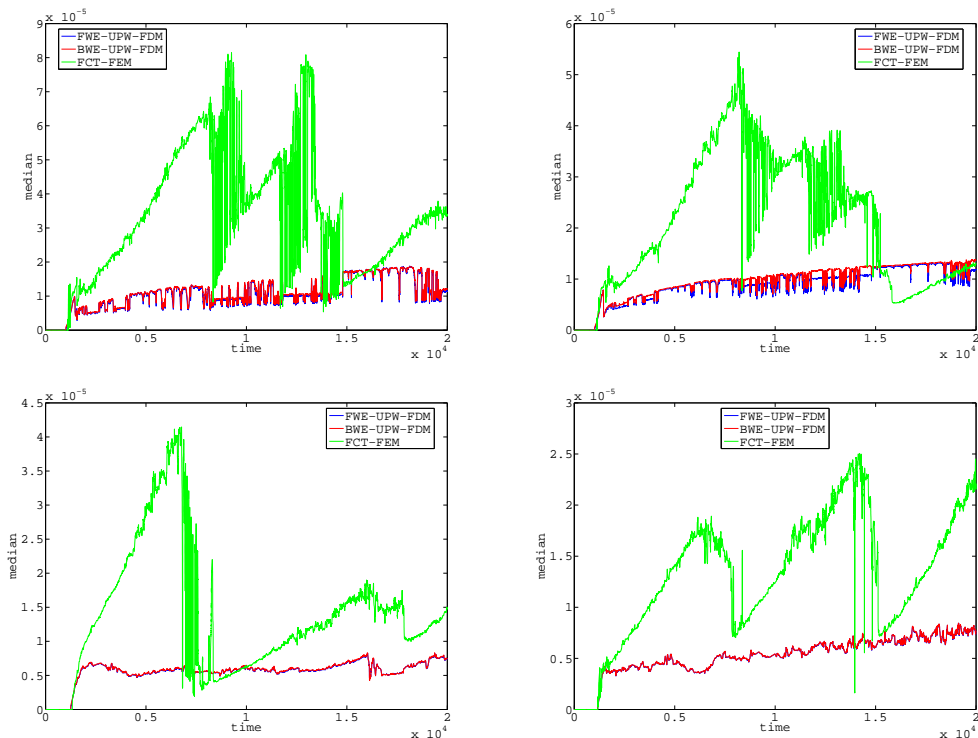


Figure 5: Evolution of the median of the volume fraction for the case  $u_\infty = 10^{-2}$ ; from top left to bottom right:  $L = 32$ ,  $\Delta t = 0.0025$  ( $\Delta \tilde{t} = 0.25$  s);  $L = 64$ ,  $\Delta t = 0.0025$  ( $\Delta \tilde{t} = 0.25$  s);  $L = 64$ ,  $\Delta t = 0.00125$  ( $\Delta \tilde{t} = 0.125$  s);  $L = 64$ ,  $\Delta t = 0.000625$  ( $\Delta \tilde{t} = 0.0625$  s).

With respect to the computing times, Table 5, the situation is essentially the same as for  $u = 10^{-3}$ . The larger times per time step for  $\Delta t = 0.000625$  in comparison with  $\Delta t = 0.00125$  are caused by the damping in the coupled multigrid preconditioner. Comparing in particular the Euler schemes, one obtains essentially the same results in considerably less time with the forward Euler scheme.

We think that in this case the losses in accuracy with the low order schemes are not acceptable. The higher order scheme FEM–FCT should be used.

Table 5: Studies with  $u_\infty = 10^{-2}$ : averaged computing time per time step in seconds.

$L$	disc. of PSD equ.	$\Delta t = 0.0025$	$\Delta t = 0.00125$	$\Delta t = 0.000625$
		$\Delta \tilde{t} = 0.25 \text{ s}$	$\Delta \tilde{t} = 0.125 \text{ s}$	$\Delta \tilde{t} = 0.0625 \text{ s}$
32	FWE–UPW–FDM	3.66	1.64	2.08
	BWE–UPW–FDM	4.57	2.40	2.79
	FEM–FCT	6.05	4.03	4.35
48	FWE–UPW–FDM	3.57	1.63	2.12
	BWE–UPW–FDM	4.96	2.77	3.10
	FEM–FCT	7.29	5.09	5.37
64	FWE–UPW–FDM	3.68	1.64	2.20
	BWE–UPW–FDM	5.11	3.11	3.37
	FEM–FCT	8.47	6.23	6.39

## 5 Summary and conclusions

The paper presented simulations of precipitation processes which are modeled with a coupled population balance system. The emphasis of the numerical studies was on different schemes for solving the higher dimensional population balance equation. Concerning the background flow, two situations have been considered: a structured flow field with small changes in time and a highly time-dependent flow field. These situations led to rather different conclusions:

- Structured flow field with small changes in time. The results with respect to the median of the volume fraction were qualitatively the same for all considered schemes for solving the population balance equation. Since the forward Euler/upwind finite difference method was by far the fastest scheme, its use might be recommended in this situation.
- Highly time-dependent flow field. The results obtained with the first order Euler/upwind finite difference schemes are qualitatively different to the results from the Crank–Nicolson FEM–FCT scheme. The smoothing effect of the first order schemes is clearly visible. Since the Crank–Nicolson FEM–FCT scheme is known to be a rather accurate scheme for strongly convection-dominated problems [18], we think that the results obtained with this scheme are more reliable. Hence, this scheme should be recommended in the case of highly time-dependent flow fields, particularly if the flow fields become turbulent as often in applications.

Our implementation of the finite difference schemes used the property that the flow domain is rectangular. On arbitrary domains, these schemes will lose certainly some efficiency whereas the FEM–FCT scheme is not affected by the shape of the flow domain.

Future studies will include the extension of the simulations to 3D flows and 4D population balance equations. An important issue will be the speed-up of the matrix assembling for the FEM–FCT scheme of the population balance equation. These studies will explore, for instance, the application of using different quadrature rules for the spatial and internal coordinates in the assembling of this matrix. In addition, a non-linear FEM–FCT scheme for the equations for the reaction and the PSD equation will be studied.

## References

- [1] M. Braack, E. Burman, V. John, and G. Lube. Stabilized finite element methods for the generalized oseen problem. *Comput. Methods Appl. Mech. Engrg.*, 196:853 – 866, 2007.
- [2] D. Chakraborty and S.K. Bhatia. Formation and aggregation of polymorphs in continuous precipitation. 2. Kinetics of  $CaCO_3$  precipitation. *Industrial & Engineering Chemistry Research*, 35:1995 – 2006, 1996.
- [3] T.A. Davis. Algorithm 832: UMFPACK V4.3—an unsymmetric-pattern multifrontal method. *ACM Trans. Math. Software*, 30:196 – 199, 2004.
- [4] R.A. Dawe and Y. Zhang. Kinetics of calcium carbonate scaling using observations from glass micromodels. *Journal of Petroleum Science and Engineering*, 18:179 – 187, 1996.
- [5] J. Gradl, H.-C. Schwarzer, F. Schwertfirm, M. Manhart, H.-J. Schmid, and W. Peukert. Precipitation of nanoparticles in a T-mixer: Coupling the particle population dynamics with hydrodynamics through direct numerical simulation. *Chem. Engrg. Proc.*, pages 908 – 916, 2007.
- [6] P.M. Gresho and R.L. Sani. *Incompressible Flow and the Finite Element Method*. Wiley, Chichester, 2000.
- [7] W. Heineken, D. Flockerzi, C. Steyer, A. Voigt, and K. Sundmacher. Nonlinear dynamics of continuous precipitation reactors: A model based analysis. *Chem. Engrg. Sci.*, 62:4896 – 4902, 2007.
- [8] T.J.R. Hughes and A.N. Brooks. A multidimensional upwind scheme with no crosswind diffusion. In T.J.R. Hughes, editor, *Finite Element*

- Methods for Convection Dominated Flows, AMD vol.34*, pages 19 – 35. ASME, New York, 1979.
- [9] V. John. Reference values for drag and lift of a two-dimensional time dependent flow around a cylinder. *Int. J. Numer. Meth. Fluids*, 44:777 – 788, 2004.
- [10] V. John. On the efficiency of linearization schemes and coupled multigrid methods in the simulation of a 3d flow around a cylinder. *Int. J. Num. Meth. Fluids*, 50:845 – 862, 2006.
- [11] V. John and P. Knobloch. A comparison of spurious oscillations at layers diminishing (sold) methods for convection–diffusion equations: Part I – a review. *Comput. Methods Appl. Mech. Engrg.*, 196:2197 – 2215, 2007.
- [12] V. John and P. Knobloch. A comparison of spurious oscillations at layers diminishing (sold) methods for convection–diffusion equations: Part II – analysis for  $P_1$  and  $Q_1$  finite elements. *Comput. Methods Appl. Mech. Engrg.*, 197:1997 – 2014, 2008.
- [13] V. John and G. Matthies. Higher order finite element discretizations in a benchmark problem for incompressible flows. *Int. J. Numer. Meth. Fluids*, 37:885 – 903, 2001.
- [14] V. John and G. Matthies. MoonNMD - a program package based on mapped finite element methods. *Comput. Visual. Sci.*, 6:163 – 170, 2004.
- [15] V. John, G. Matthies, and J. Rang. A comparison of time–discretization/linearization approaches for the time–dependent incompressible Navier–Stokes equations. *Comput. Methods Appl. Mech. Engrg.*, 195:5995 – 6010, 2006.
- [16] V. John, T. Mitkova, M. Roland, K. Sundmacher, L. Tobiska, and A. Voigt. Simulations of population balance systems with one internal coordinate using finite element methods. *Chem. Engrg. Sci.*, 2008. in press.
- [17] V. John and E. Schmeier. On finite element methods for 3d time–dependent convection–diffusion–reaction equations with small diffusion. In *Proceedings of the BAIL conference, Limerick 2008*, 2008. in press.
- [18] V. John and E. Schmeier. Stabilized finite element methods for time–dependent convection–diffusion–reaction equations. *Comput. Methods Appl. Mech. Engrg.*, 198:475 – 494, 2008.

- [19] V. Kulikov, H. Briesen, R. Grosch, L. von Wedel, A. Yang, and W. Marquardt. Modular dynamic simulation for integrated particulate processes by means of tool integration. *Chem. Engrg. Sci.*, 60:2069 – 2083, 2005.
- [20] V. Kulikov, H. Briesen, and W. Marquardt. A framework for the simulation of mass crystallization considering the effect of fluid dynamics. *Chem. Engrg. Proc.*, 60:886 – 899, 2007.
- [21] D. Kuzmin. Explicit and implicit FEM–FCT algorithms with flux linearization. *Ergebnisberichte Angew. Math.* 358, University of Dortmund, 2008.
- [22] D. Kuzmin and M. Möller. Algebraic flux correction I. Scalar conservation laws. In R. Löhner D. Kuzmin and S. Turek, editors, *Flux-Corrected Transport: Principles, Algorithms and Applications*, pages 155 – 206. Springer, 2005.
- [23] D. Kuzmin, M. Möller, and S. Turek. High-resolution FEM–FCT schemes for multidimensional conservation laws. *Comput. Methods Appl. Mech. Engrg.*, 193:4915 – 4946, 2004.
- [24] R.J. LeVeque. *Numerical methods for conservation laws*. Lecture Notes in Mathematics, ETH Zürich. Birkhäuser Verlag Basel, 2nd edition, 1992.
- [25] G. Matthies, P. Skrzypacz, and L. Tobiska. A unified convergence analysis for local projection stabilisations applied to the Oseen problem. *M2AN*, 41:713 – 742, 2007.
- [26] S. B. Pope. *Turbulent flows*. Cambridge University Press, 2000.
- [27] D. Ramkrishna. *Population Balances: Theory and Applications to Particulate Systems in Engineering*. Academic Press, San Diego, 2000.
- [28] H.-G. Roos, M. Stynes, and L. Tobiska. *Robust Numerical Methods for Singularly Perturbed Differential Equations*, volume 24 of *Springer Series in Computational Mathematics*. Springer, 2nd edition, 2008.
- [29] Y. Saad. *Iterative methods for sparse linear systems*. SIAM Philadelphia, 2nd edition, 2003.
- [30] H.-C. Schwarzer, F. Schwertfirm, M. Manhart, H.-J. Schmid, and W. Peukert. Predictive simulation of nanoparticle precipitation based on the population balance equation. *Chem. Engrg. Sci.*, pages 167 – 181, 2006.

- [31] R.A. Shaw. Particle–turbulence interactions in atmospheric clouds. *Annu. Rev. Mech.*, 35:183 – 227, 2003.
- [32] M. Tabata. A finite element approximation corresponding to the upwind differencing. *Memoirs of Numerical Mathematics*, 1:47 – 63, 1977.
- [33] N.S. Tavaré and J. Garside. *Industrial Crystallization: Process Simulation Analysis and Design*. The Plenum Chemical Engineering Series. Plenum Press New York and London, 1995.
- [34] D. Verdoes, D. Kashchiev, and G.M. van Rosmalen. Determination of nucleation and growth rates from induction times in seeded and unseeded precipitations of calcium carbonate. *Journal of Crystal Growth*, 118:401 – 413, 1992.
- [35] S.T. Zalesak. Fully multi-dimensional flux corrected transport algorithms for fluid flow. *J. Comput. Phys.*, 31:335 – 362, 1979.